Au(III)-proline derivatives exhibiting selective antiproliferative activity against HepG2/SB3 apoptosis-resistant cancer cells

Leonardo Brustolin,[a][b] Nicolò Pettenuzzo,[a][b] Chiara Nardon,[a] Santina Quarta,[c] Luciano Marchiò,[d] Barbara Biondi[e], Patrizia Pontisso,[c] and Dolores Fregona*[a]

[a] Department of Chemical Sciences, University of Padova,Via F. Marzolo 1, 35131 Padova (Italy)

[b] Department of Chirurgic, Oncologic and Gastroenterological Sciences,University of Padova, Via Giustiniani 2, 35128, Padova (Italy)

[c] Department of Medicine, University of Padova, Via Giustiniani 2, 35128, Padova (Italy)

[d] Department of Chemical Sciences, Life Sciences and Environmental Sustainability, University of Parma, Parco Area delle Scienze 11/a, 43124, Parma (Italy)

[e] CNR, Padova Unit, Inst Biomol Chem, Via Marzolo 1, I-35131 Padua, Italy

*Author to whom correspondence may be addressed: dolores.fregona@unipd.it

X-ray crystallographic parameters

	[$AuCl_2$(ProO*t*BuDTC)] (4)	**[$AuBr_2$(ProOMeDTC)] (5)**	**[$AuBr_2$(ProO*t*BuDTC)] (6)**
Empirical formula	$C_{10}H_{16}AuCl_2NO_2S_2$	$C_7H_{10}AuBr_2NO_2S_2$	$C_{10}H_{16}AuBr_2NO_2S_2$
Formula weight	514.22	561.07	603.14
Temperature/K	200(2)	293(2)	293(2)
Crystal system	monoclinic	orthorhombic	monoclinic
Space group	$P2_1$	$P2_12_12_1$	$P2_1$
a/Å	6.8275(2)	7.197(2)	6.985(2)
b/Å	22.0294(7)	14.315(3)	22.283(7)
c/Å	10.7863(3)	26.370(5)	11.048(3)

α/°	90	90	90
β/°	101.659(1)	90	102.358(5)
γ/°	90	90	90
Volume/Å^3	1588.85(8)	2716.8(11)	1679.7(8)
Z	4	8	4
ρ_{calc}g/cm^3	2.150	2.743	2.385
μ/mm^{-1}	9.851	17.001	13.758
F(000)	976.0	2048.0	1120.0
Crystal size/mm^3	0.21 × 0.16 × 0.06	0.42 × 0.12 × 0.10	0.28 × 0.05 × 0.05
2Θ range (°)	6.368 to 52.058	3.088 to 51.696	3.656 to 51.998
Reflections collected/unique	22908/6215	31186/5231	14950/6537
Data/restraints/ parameters	6215/2/331	5231/0/273	6537/1/331
Goodness-of-fit on F^2	0.919	1.009	0.946
R_1 [I>=2σ (I)]	0.0173	0.0369	0.0436
wR_2 [I>=2σ (I)]	0.0352	0.0783	0.0805
Flack parameter	0.011(4)	0.021(8)	-0.002(12)

Table SI 1 Summary of X-ray crystallographic data for [$AuBr_2$(ProOMeDTC)] (**4**), [$AuCl_2$(ProO*t*BuDTC)] (**5**), [$AuBr_2$(ProO*t*BuDTC)] (**6**).

$R1 = \Sigma||F_O|-|F_C||/\Sigma|F_O|$, $wR2 = [\Sigma[w(F_O^2-F_C^2)^2]/\Sigma[w(F_O^2)^2]]^{½}$, $w = 1/[\sigma^2(F_O^2) + (aP)^2 + bP]$, where $P = [\max(F_O^2,0) + 2F_C^2]/3$.

[$AuCl_2$(ProO*t*BuDTC)] (4)		[$AuBr_2$(ProOMeDTC)] (5)		[$AuBr_2$(ProOMeDTC)] (4)	
Au(1)-S(11)	2.309(2)	Au(1)-S(11)	2.316(4)	Au(1)-S(11)	2.323(5)
Au(1)-S(21)	2.294(2)	Au(1)-S(21)	2.315(4)	Au(1)-S(21)	2.305(5)
Au(1)-Cl(1)	2.311(2)	Au(1)-Br(1)	2.436(2)	Au(1)-Br(1)	2.441(2)
Au(1)-Cl(2)	2.307(2)	Au(1)-Br(2)	2.435(2)	Au(1)-Br(2)	2.436(2)
Au(2)-S(12)	2.298(2)	Au(2)-S(12)	2.301(4)	Au(2)-S(12)	2.314(5)
Au(2)-S(22)	2.305(2)	Au(2)-S(22)	2.324(4)	Au(2)-S(22)	2.315(5)
Au(2)-Cl(3)	2.311(2)	Au(2)-Br(3)	2.441(2)	Au(2)-Br(3)	2.435(2)
Au(2)-Cl(4)	2.300(2)	Au(2)-Br(4)	2.441(2)	Au(2)-Br(4)	2.427(2)

Table SI 2 Selected geometric parameters (Å) for [$AuCl_2$(ProO*t*BuDTC)] (**4**), [$AuBr_2$(ProOMeDTC)] (**5**), [$AuBr_2$(ProO*t*BuDTC)] (**6**).

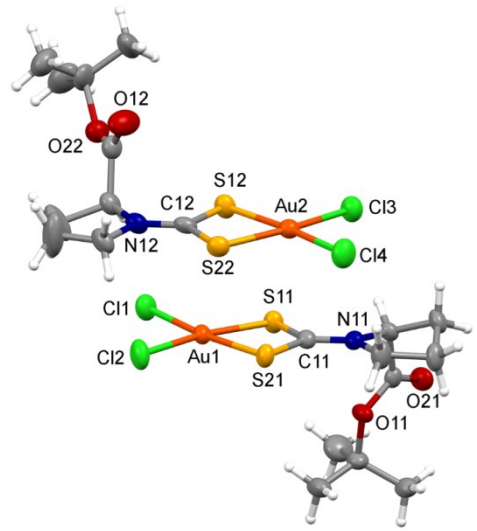

Fig. SI 1 Molecular structure of the complex **4** with thermal ellipsoids drawn at the **50% probability** level. Both molecular entities within the asymmetric unit are shown. CCDC 1845775.

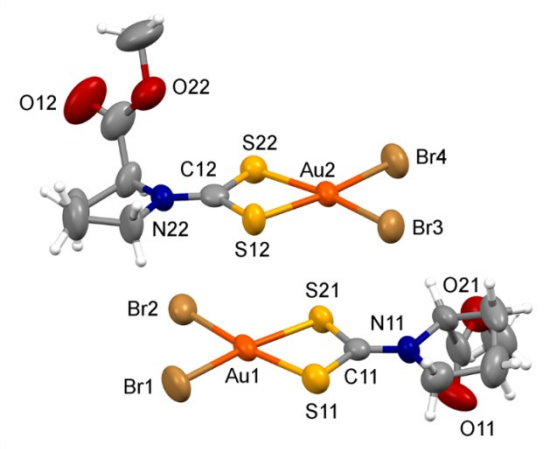

Fig. SI 2 Molecular structure of the complex **5** with thermal ellipsoids drawn at the **50% probability** level. Both molecular entities within the asymmetric unit are shown. CCDC 1845776.

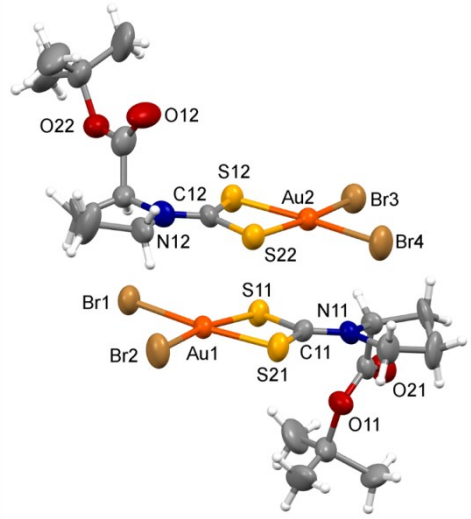

Fig. SI 3 Molecular structure of the complex **6** with thermal ellipsoids drawn at the **50% probability** level. Both molecular entities within the asymmetric unit are shown. CCDC 1845777.

IR spectra

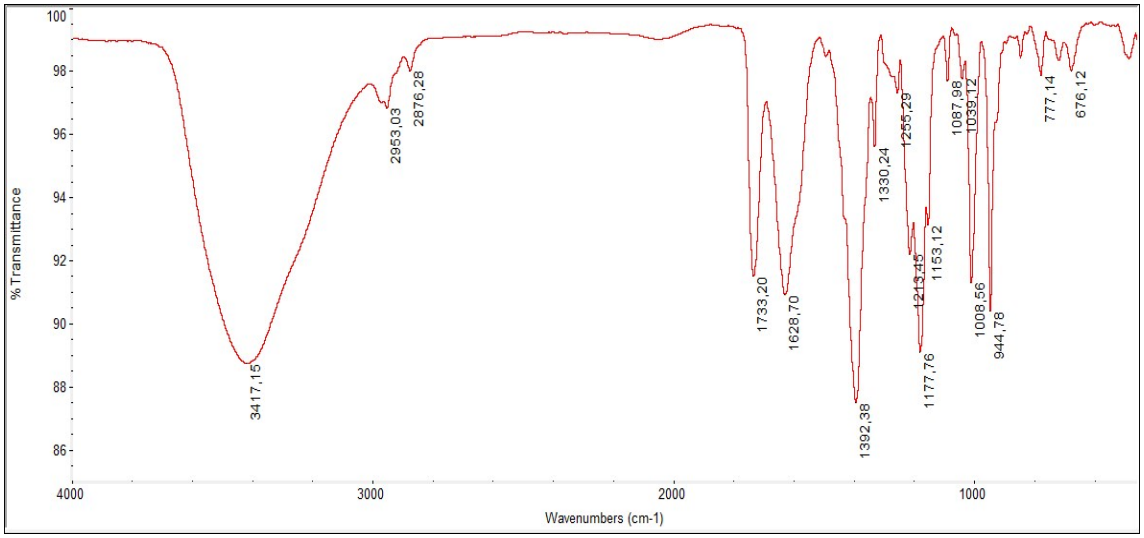

Fig. SI 4 Medium FT-IR (4000-500 cm^{-1}, KBr) spectrum of L-proline methyl ester dithiocarbamate sodium salt (Na ProOMeDTC).

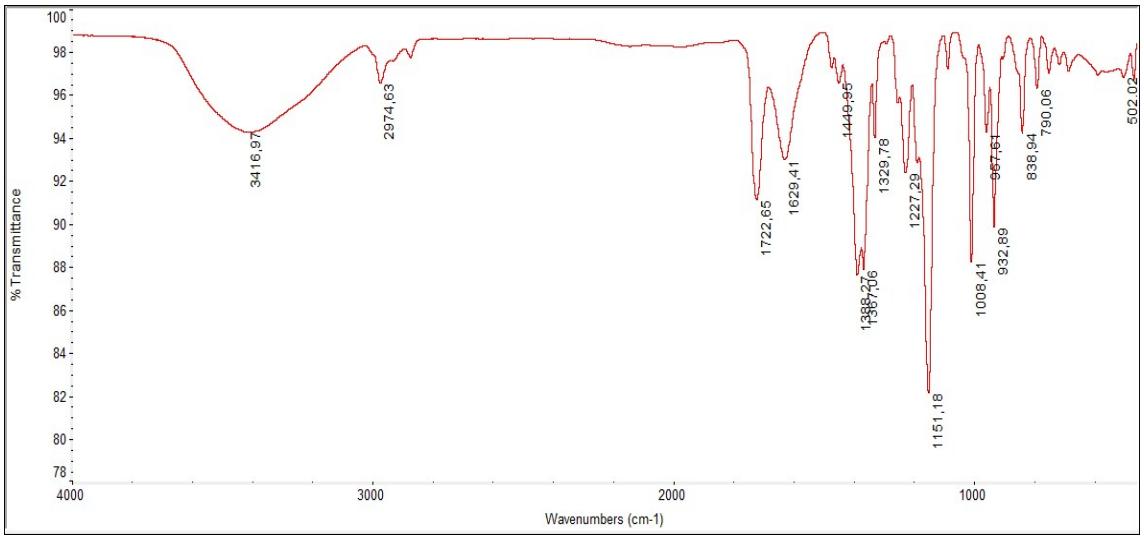

Fig. SI 5 Medium FT-IR (4000-500 cm^{-1}, KBr) spectrum of L-proline *tert*-butyl ester dithiocarbamate sodium salt (Na ProO*t*BuDTC).

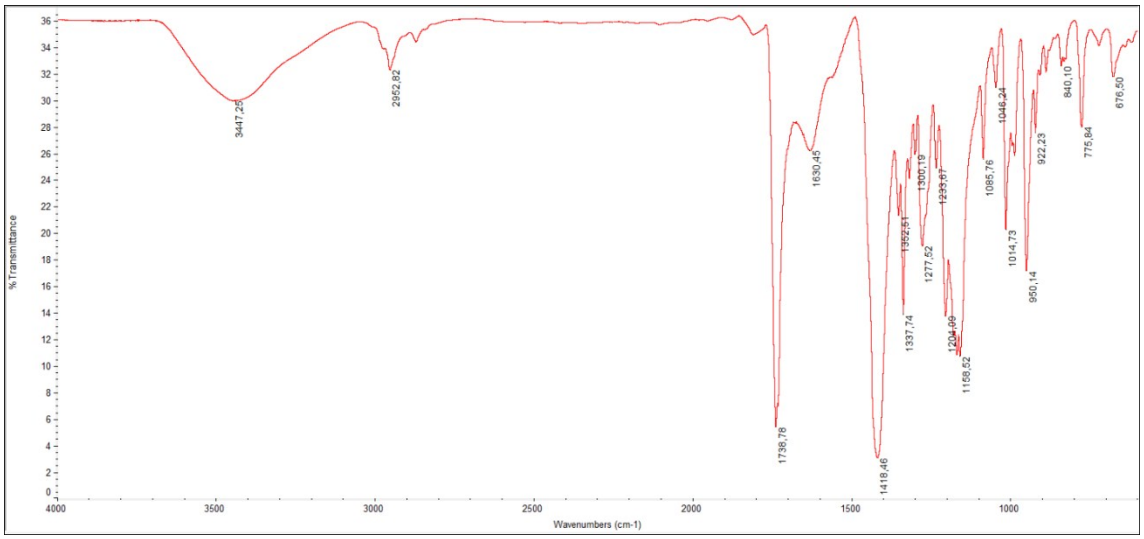

Fig. SI 6 Medium FT-IR (4000-600 cm^{-1}, KBr) spectrum of bis(L-proline methyl ester dithiocarbamate)digold(I), $[Au_2(ProOMeDTC)_2]$ (**1**).

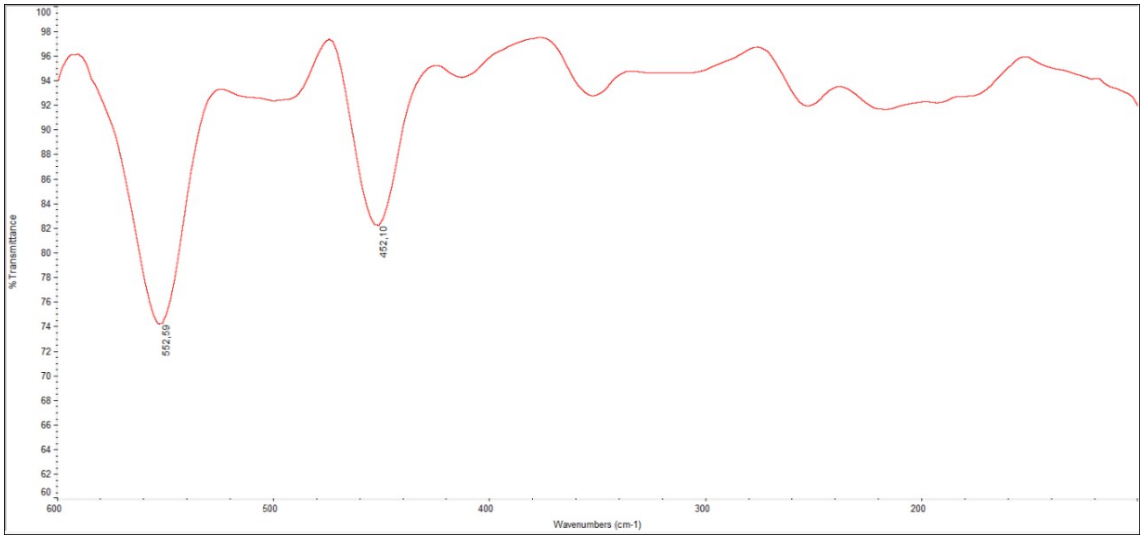

Fig. SI 7 Far FT-IR (600-100 cm^{-1}, nujol) spectrum of bis(L-proline methyl ester dithiocarbamate)digold(I), $[Au_2(ProOMeDTC)_2]$ (**1**).

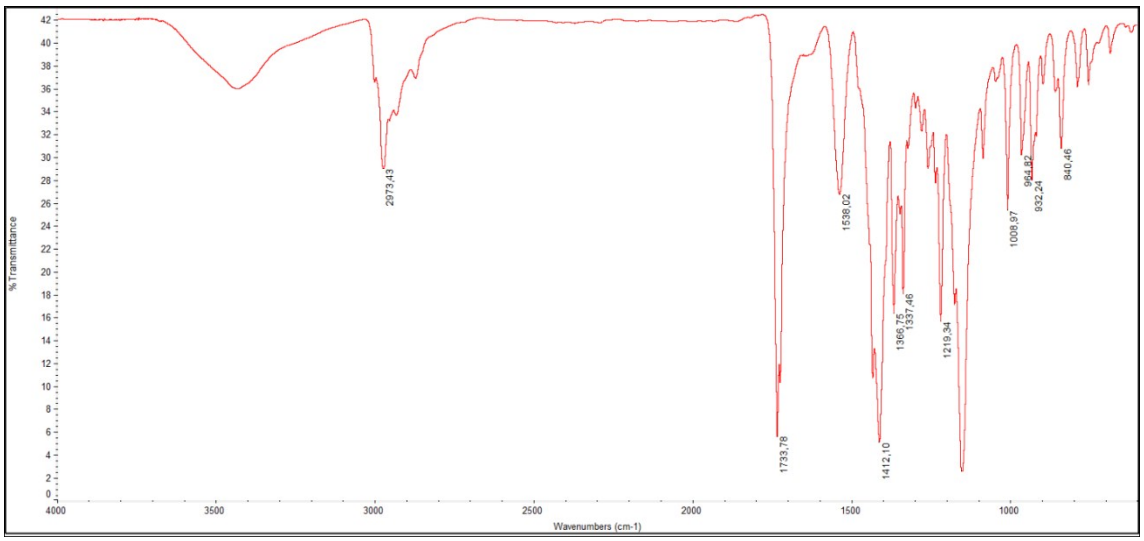

Fig. SI 8 Medium FT-IR (4000-600 cm^{-1}, KBr) spectrum of bis(L-proline *tert*-butyl ester dithiocarbamate)digold(I), $[Au_2(ProO\mathit{t}BuDTC)_2]$ (**2**).

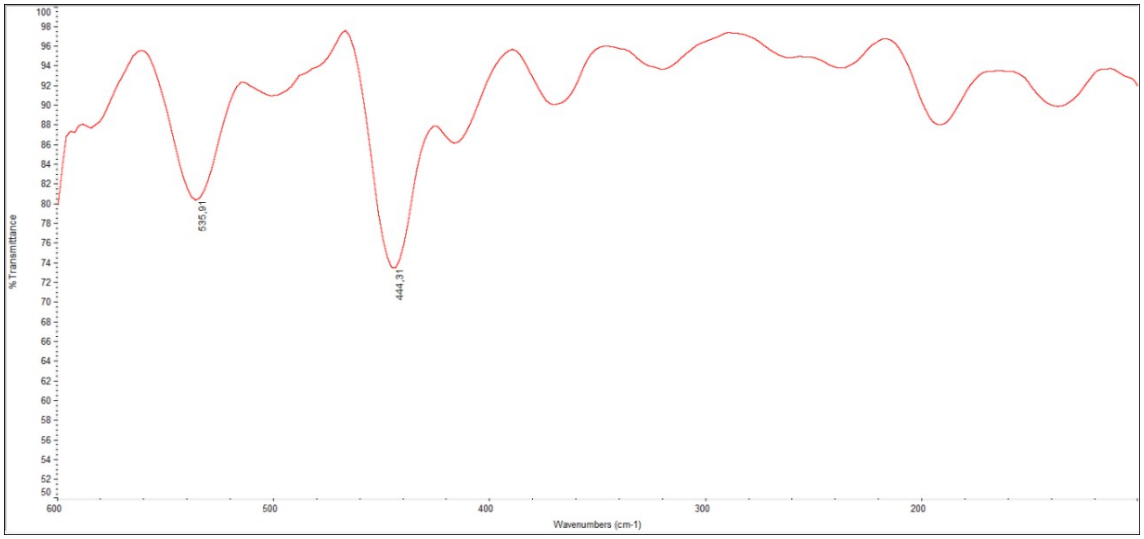

Fig. SI 9 Far FT-IR (600-100 cm^{-1}, nujol) spectrum of bis(L-proline *tert*-butyl ester dithiocarbamate)digold(I), $[Au_2(ProO\mathit{t}BuDTC)_2]$ (**2**).

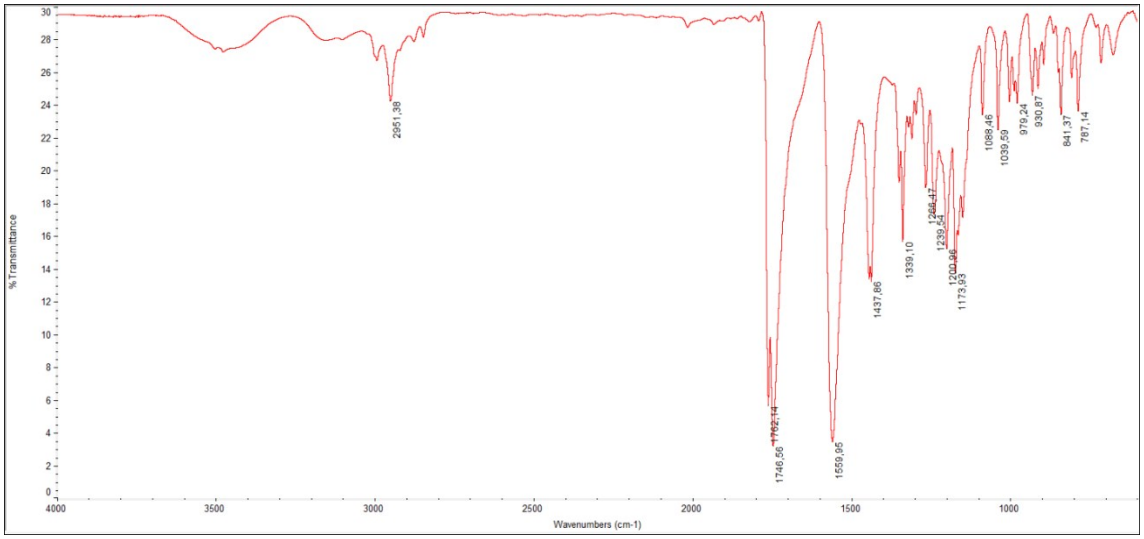

Fig. SI 10 Medium FT-IR (4000-600 cm^{-1}, KBr) spectrum of dichloro(L-proline methyl ester dithiocarbamate)gold(III), $[AuCl_2(ProOMeDTC)]$ (**3**).

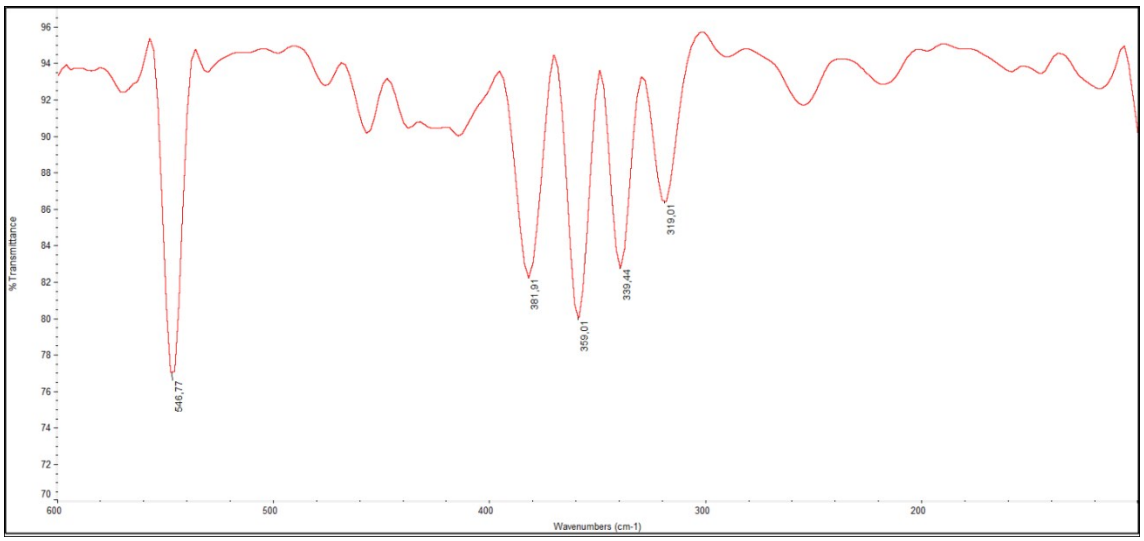

Fig. SI 11 Far FT-IR (600-100 cm^{-1}, nujol) spectrum of dichloro(L-proline methyl ester dithiocarbamate)gold(III), $[AuCl_2(ProOMeDTC)]$ (**3**).

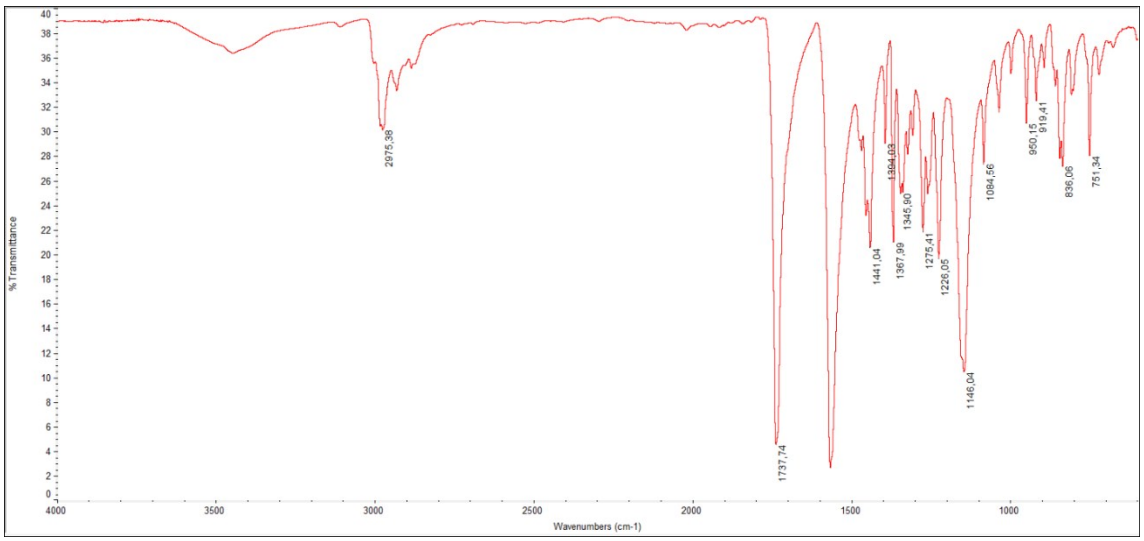

Fig. SI 12 Medium FT-IR (4000-600 cm^{-1}, KBr) spectrum of dichloro(L-proline *tert*-butyl ester dithiocarbamate)gold(III), [$AuCl_2$(ProO*t*BuDTC)] (**4**).

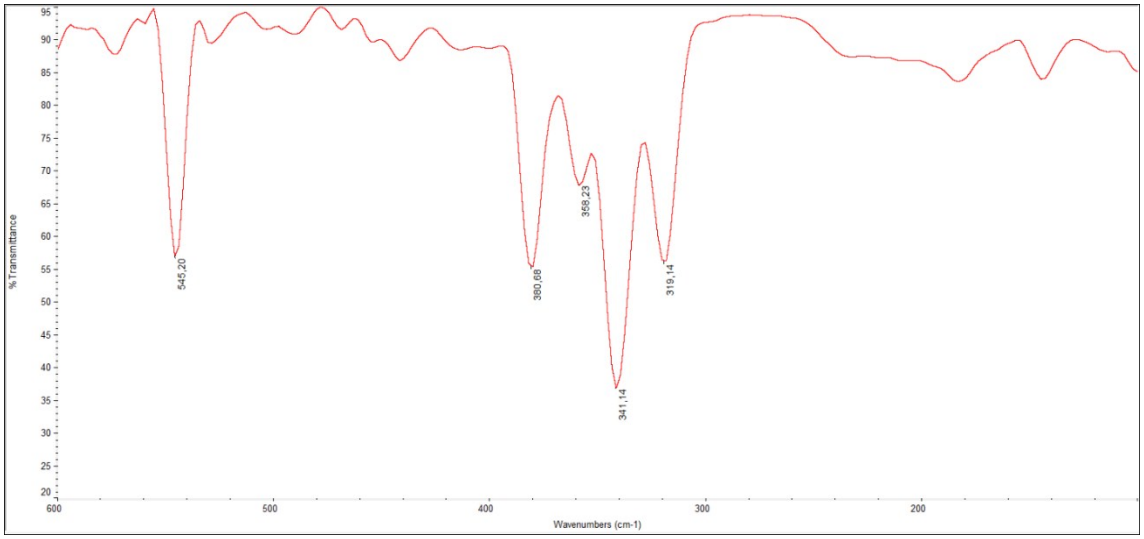

Fig. SI 13 Far FT-IR (600-100 cm^{-1}, nujol) spectrum of dichloro(L-proline *tert*-butyl ester dithiocarbamate)gold(III), [$AuCl_2$(ProO*t*BuDTC)] (**4**).

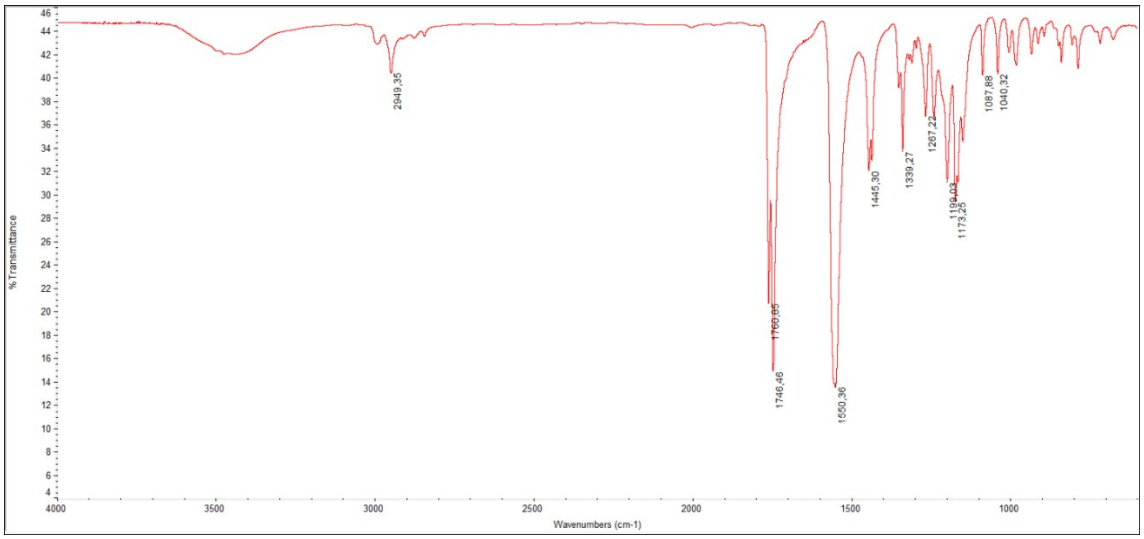

Fig. SI 14 Medium FT-IR (4000-600 cm^{-1}, KBr) spectrum of dibromo(L-proline methyl ester dithiocarbamate)gold(III), [$AuBr_2$(ProOMeDTC)] (**5**).

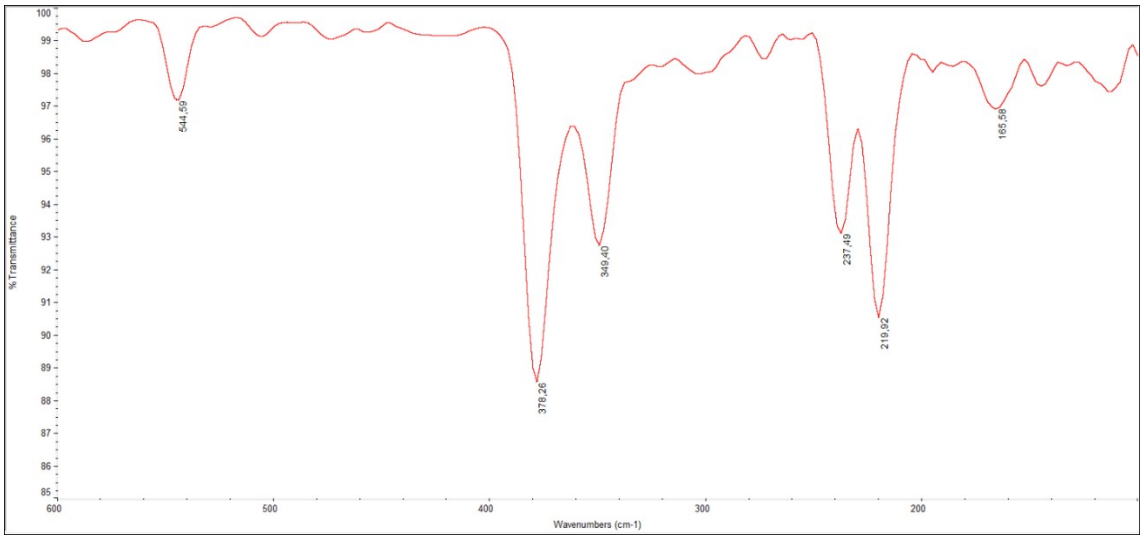

Fig. SI 15 Far FT-IR (600-100 cm^{-1}, nujol) spectrum of dibromo(L-proline methyl ester dithiocarbamate)gold(III), [$AuBr_2$(ProOMeDTC)] (**5**).

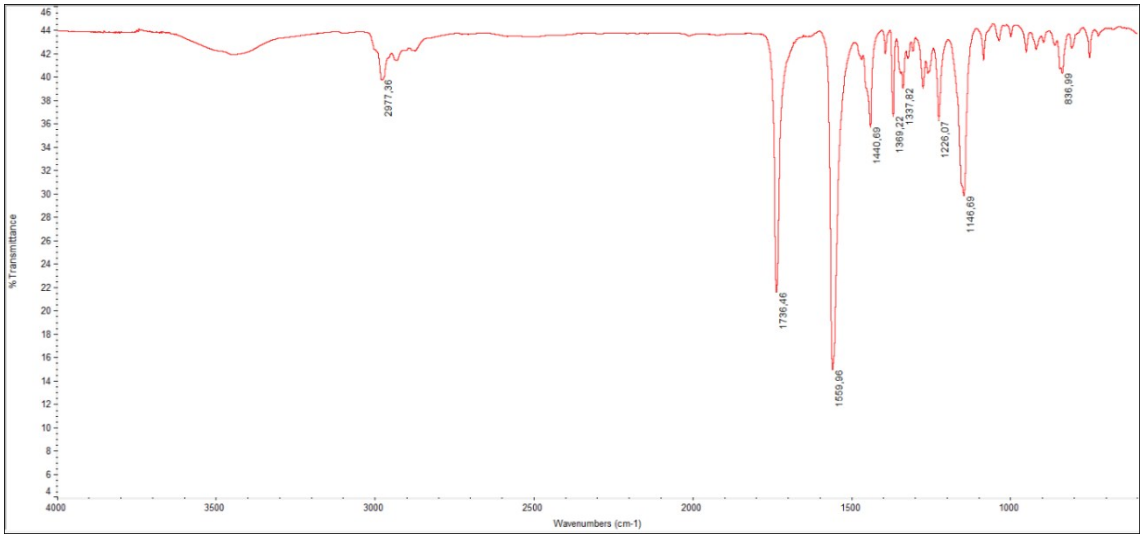

Fig. SI 16 Medium FT-IR (4000-600 cm^{-1}, KBr) spectrum of dibromo(L-proline *tert*-butyl ester dithiocarbamate)gold(III), [$AuBr_2$(ProO*t*BuDTC)] (**6**).

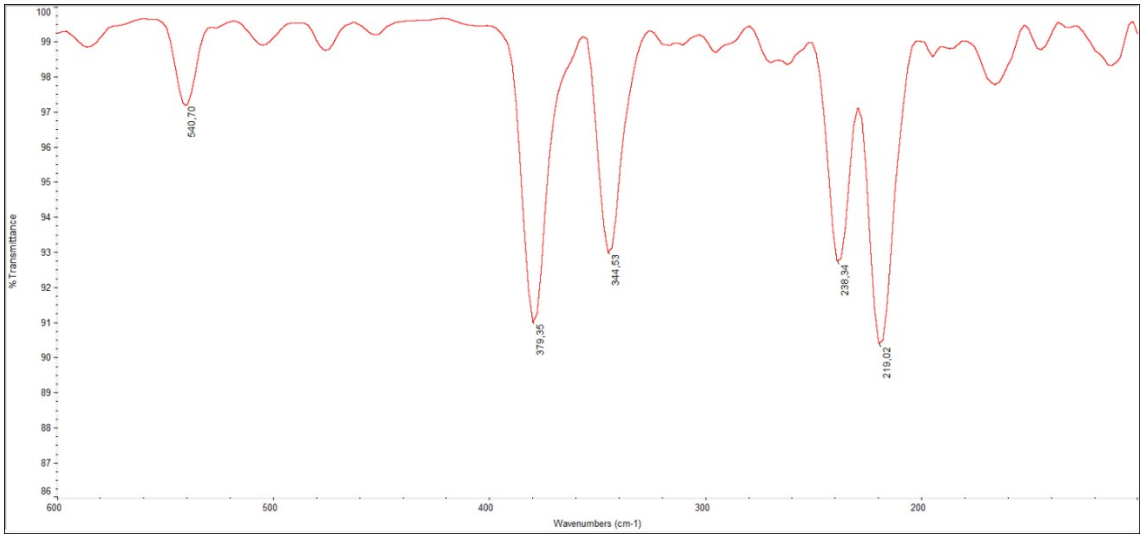

Fig. SI 17 Far FT-IR (600-100 cm^{-1}, nujol) spectrum of dibromo(L-proline *tert*-butyl ester dithiocarbamate)gold(III), [$AuBr_2$(ProO*t*BuDTC)] (**6**).

^{1}H-NMR spectra

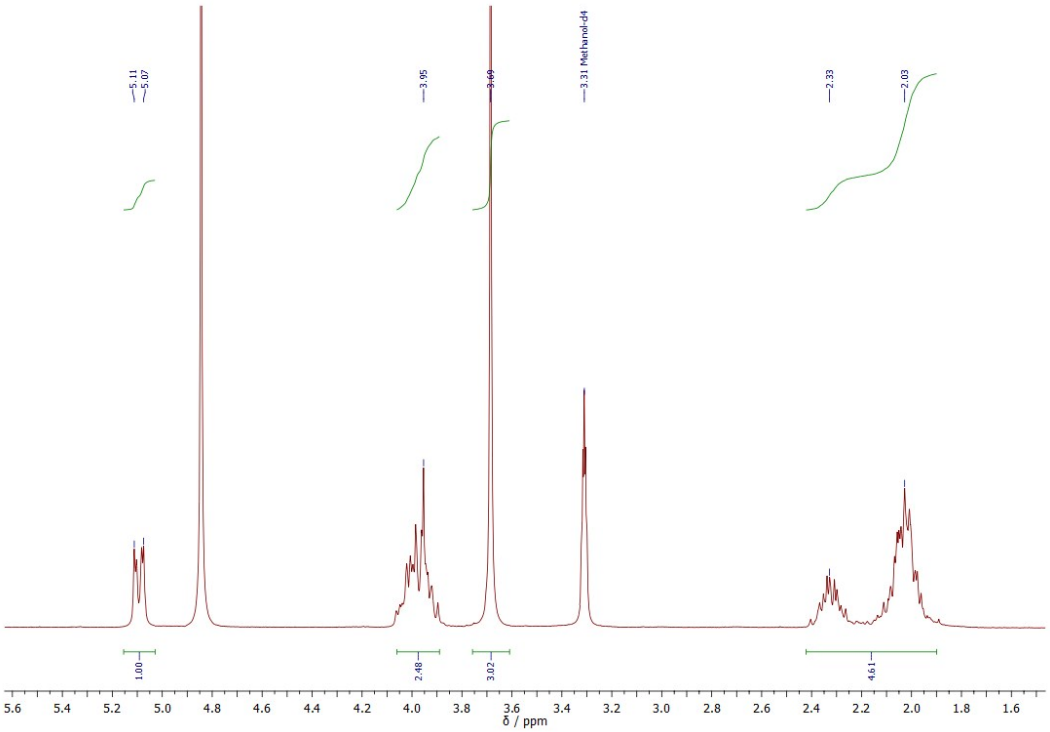

Fig. SI 18 ^{1}H-NMR (CD_3OD, 25 °C, 300.13 MHz) spectrum of L-proline methyl ester dithiocarbamate sodium salt (Na ProOMeDTC).

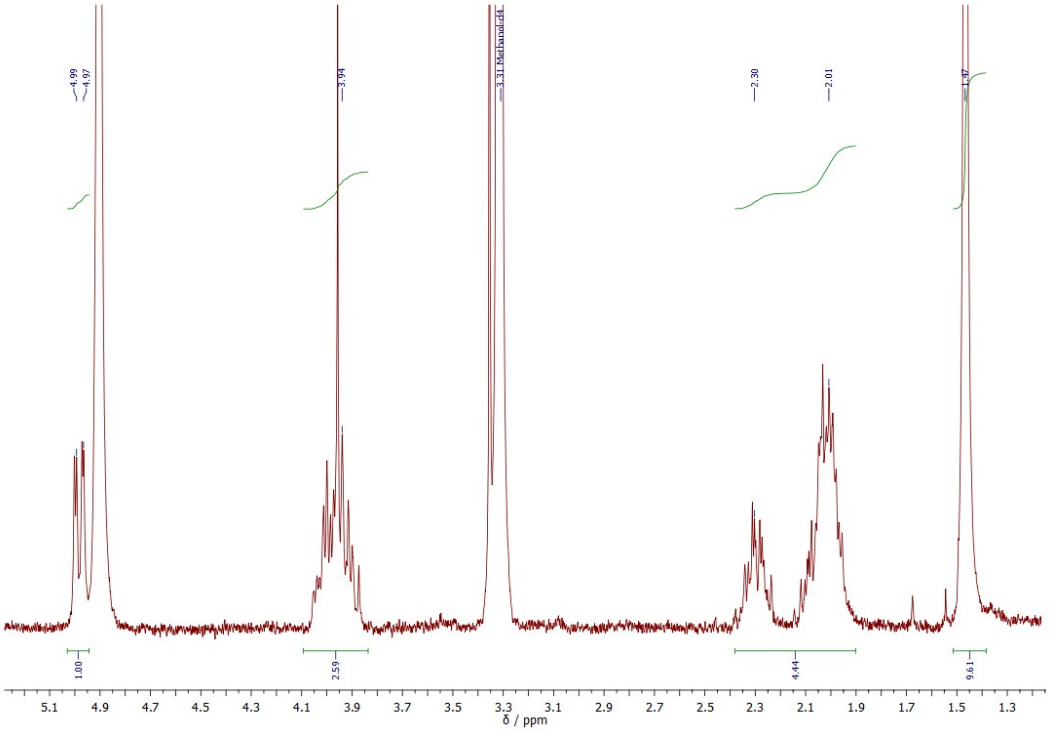

Fig. SI 19 ^{1}H-NMR (CD_3OD, 25 °C, 300.13 MHz) spectrum of L-proline *tert*-butyl ester dithiocarbamate sodium salt (Na ProO*t*BuDTC).

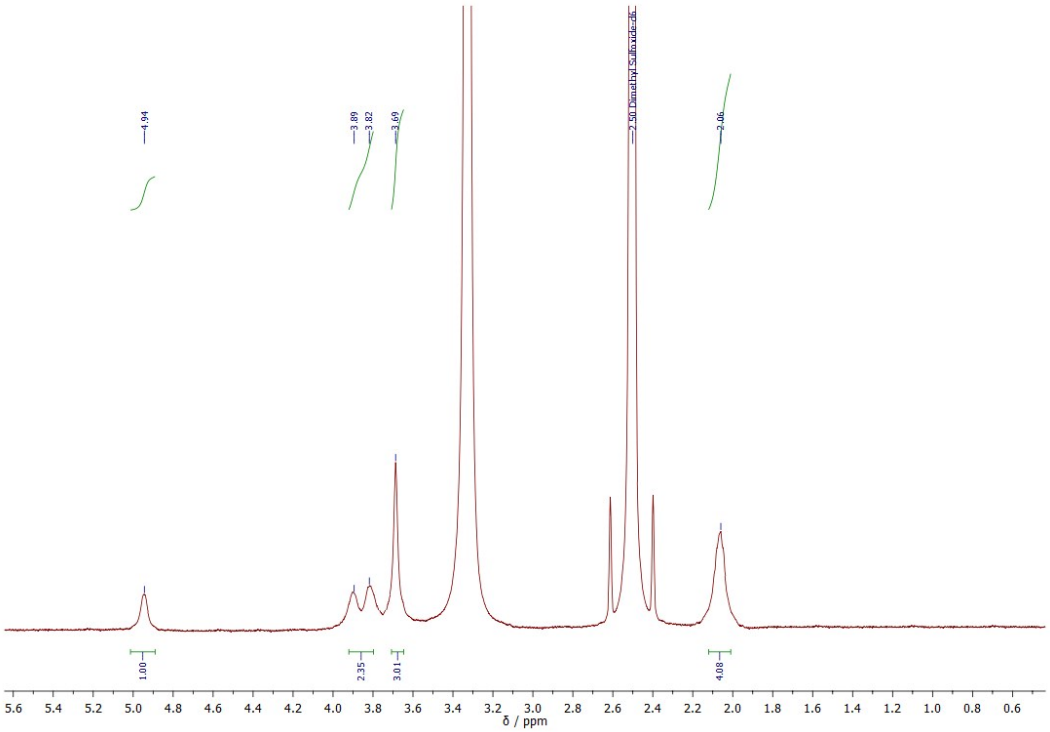

Fig. SI 20 ^{1}H-NMR (DMSO-d_6, 25 °C, 300.13 MHz) spectrum of bis(L-proline methyl ester dithiocarbamate)digold(I), [Au_2(ProOMeDTC)$_2$] (**1**).

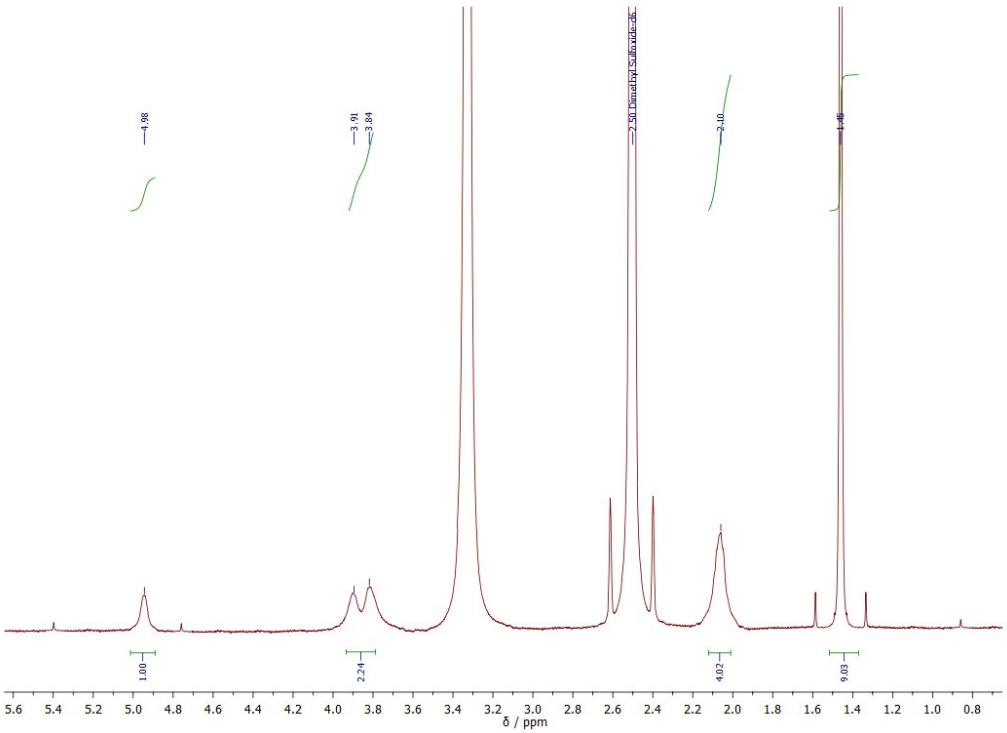

Fig. SI 21 ^{1}H-NMR (DMSO-d_6, 25 °C, 300.13 MHz) spectrum of bis(L-proline *tert*-butyl ester dithiocarbamate)digold(I), [Au_2(ProO*t*BuDTC)$_2$] (**2**).

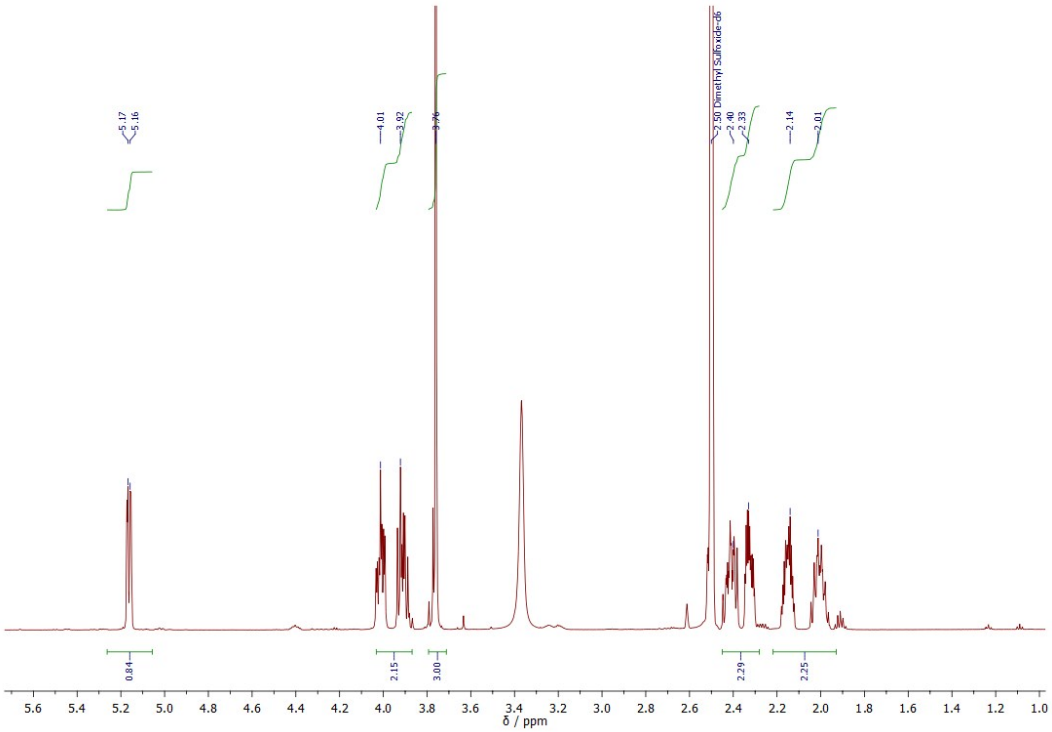

Fig. SI 22 ^{1}H-NMR (DMSO-d_6, 25 °C, 300.13 MHz) spectrum of dichloro(L-proline methyl ester dithiocarbamate)gold(III), [$AuCl_2$(ProOMeDTC)] (**3**).

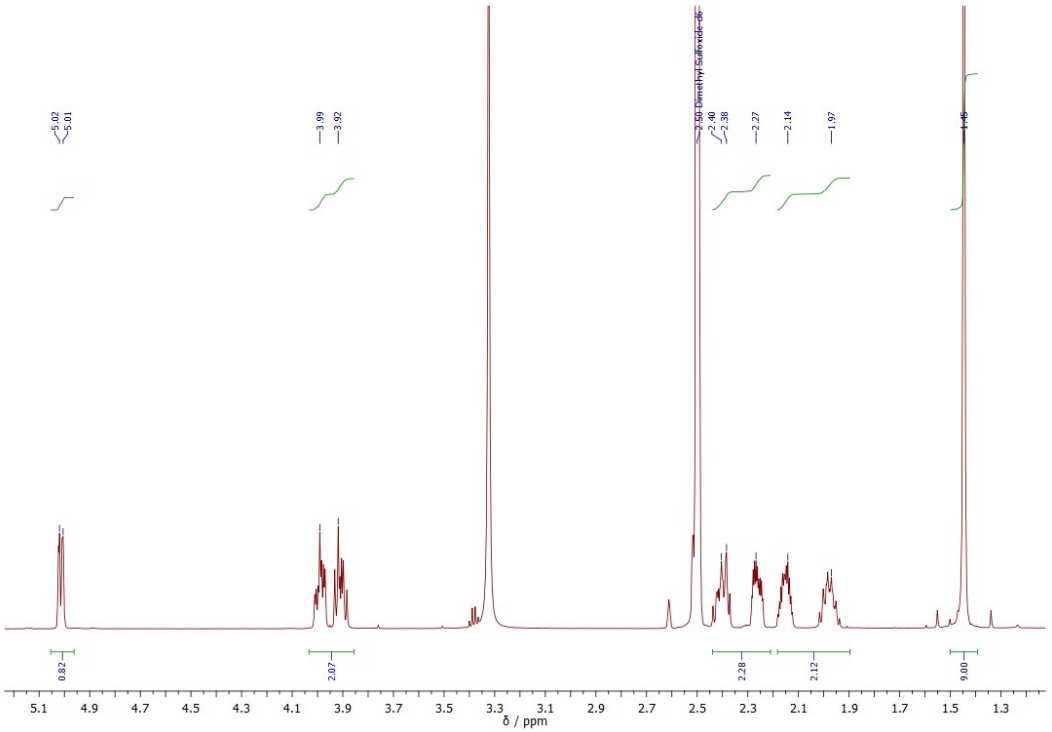

Fig. SI 23 ^{1}H-NMR (DMSO-d_6, 25 °C, 300.13 MHz) spectrum of dichloro(L-proline *tert*-butyl ester dithiocarbamate)gold(III), [$AuCl_2$(ProO*t*BuDTC)] (**4**).

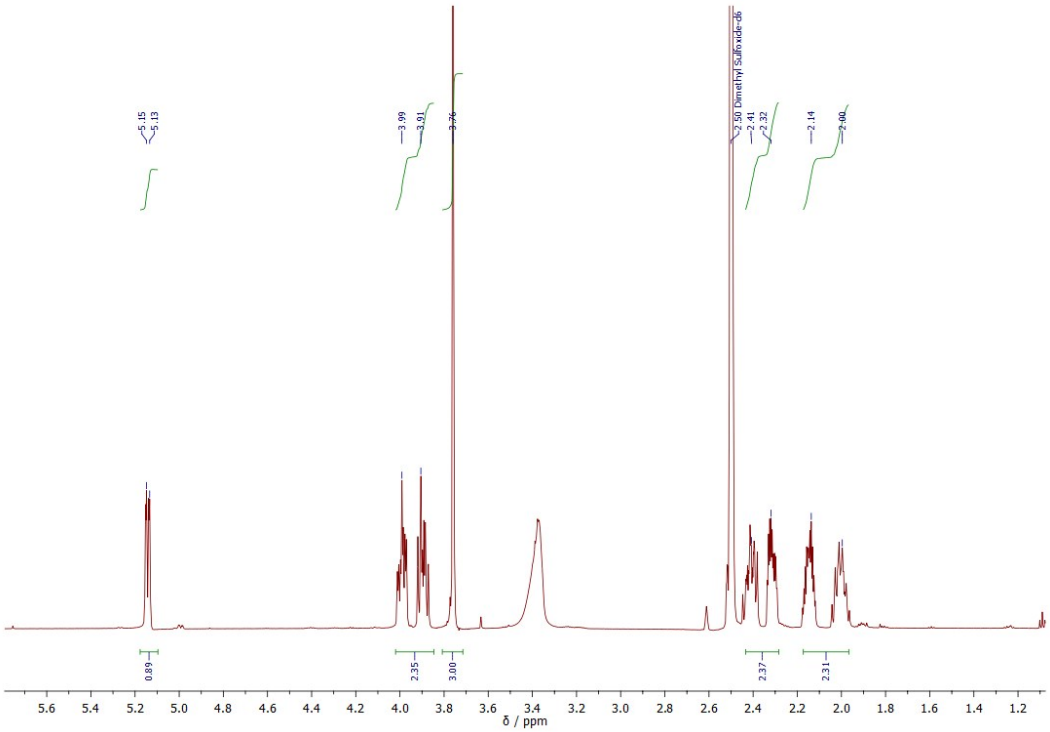

Fig. SI 24. ^{1}H-NMR (DMSO-d_6, 25 °C, 300.13 MHz) spectrum of dibromo(L-proline methyl ester dithiocarbamate)gold(III), [$AuBr_2$(ProOMeDTC)] (**5**).

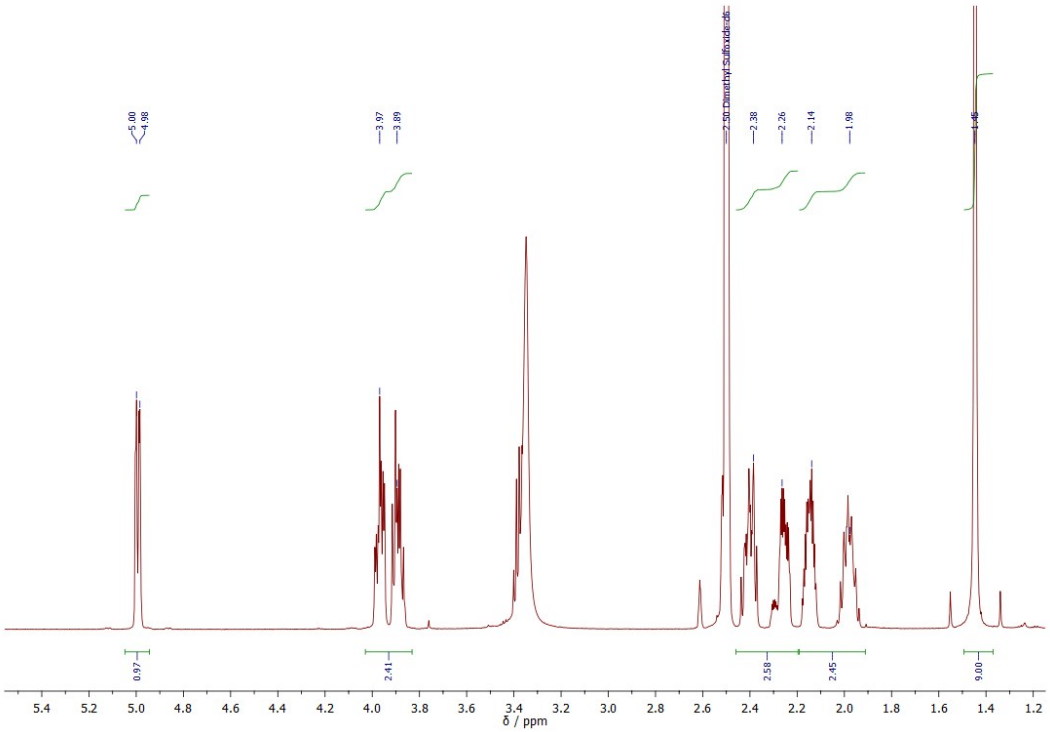

Fig. SI 25 ^{1}H-NMR (DMSO-d_6, 25 °C, 300.13 MHz) spectrum of dibromo(L-proline *tert*-butyl ester dithiocarbamate)gold(III), [$AuBr_2$(Pro*Ot*BuDTC)] (**6**).

UV-Vis studies

Compound	*band I*	*band II*	*band III*	*band IV*	*band V*
1	-	284 nm (33581)	326 nm (3382)	-	-
2	-	284 nm (39678)	324 nm (8314)	-	-
3	n.d.	n.d.	265 nm (27612)	330 nm (2818)	420 nm (329)
4	n.d.	n.d.	266 nm (29922)	330 nm (3167)	414 nm (334)
5	255 nm (25328)	271 nm (27060)	285 nm (28648)	388 nm (2310)	437 nm (1268)
6	256 nm (24339)	269 nm (25699)	284 nm (28305)	388 nm (2323)	439 nm (1194)

Table SI 3 UV-Vis spectral data (800-235 nm) of complexes **1** and **2** in DMSO and **3**-**6** recorded in CH_2Cl_2 at 25 °C. *n.d.* stands for "not detected".

The summary of the bands is highlighted in **Table SI 3** and the spectra are reported in the following **Fig. SI 26-31.** In literature, the bands I, II and III have not been undoubtedly ascribed to a particular electronic transition, since they could be assigned to either an intra-ligand π*←π transition located in the -NCSS moiety or an intra-ligand p←d transition between levels originated by sulfur atoms.[36] Moreover, concerning the Au(I)-DTC derivatives, some papers associate the band III with a ligand-to-metal charge transfer (LMCT).[37] In these dinuclear complexes which involve an Au(I)-Au(I) interaction, metal-centered transitions are foreseen at low energy (range 300-350 nm), due to the destabilization of the highest occupied d orbitals of gold (which become antibonding).[38]

The discussion on bands IV and V of Au(III) derivatives is based on the Gray and Ballhausen's description of the molecular orbital theory for SP complexes, which discerns two distinct cases.[39] The first is related to SP compounds in which the ligands themselves have a π-orbital system, whereas the second is associated with SP complexes with no intra-ligand π-orbital system. For both cases, there are three spin-allowed d-d transitions, corresponding to the one-electron transitions $^1A_{1g}\rightarrow{}^1A_{2g}$, $^1A_{1g}\rightarrow{}^1B_{1g}$ and $^1A_{1g}\rightarrow{}^1E_g$. Moreover, considering DTC ligands as moieties containing a π-orbital system, three charge-transfer (CT) transitions are foreseen, namely $^1A_{1g}\rightarrow{}^1E_u$, $^1A_{1g}\rightarrow{}^1A_{2u}$, and $^1A_{1g}\rightarrow{}^1B_{1u}$. However, only the first and second are allowed, with the $^1A_{1g}\rightarrow{}^1E_u$ transition expected to have considerably greater intensity. On the other hand, halido ligands belong to the second case presented, and in general generate two allowed CT transitions of the type $^1A_{1g}\rightarrow{}^1E_u$ (more intense) and $^1A_{1g}\rightarrow{}^1A_{2u}$.[39-41] In general, the band IV is attributed to either an intramolecular L←M charge transfer, involving the Au 5d orbitals and the dithiocarbamato π*-system (first case abovementioned), or an electron transfer of the type u←g from a 4p orbital of the halide ligands to the lowest unfilled 5d orbital (second case).[42] The band V is a weak absorption and it is easily detected in dibromido derivatives since it appears as a shoulder of the CT transition (band IV). It is attributable to the three allowed d-d transitions $^1A_{1g}\rightarrow{}^1A_{2g}$, $^1A_{1g}\rightarrow{}^1B_{1g}$ and $^1A_{1g}\rightarrow{}^1E_g$.[41, 43]

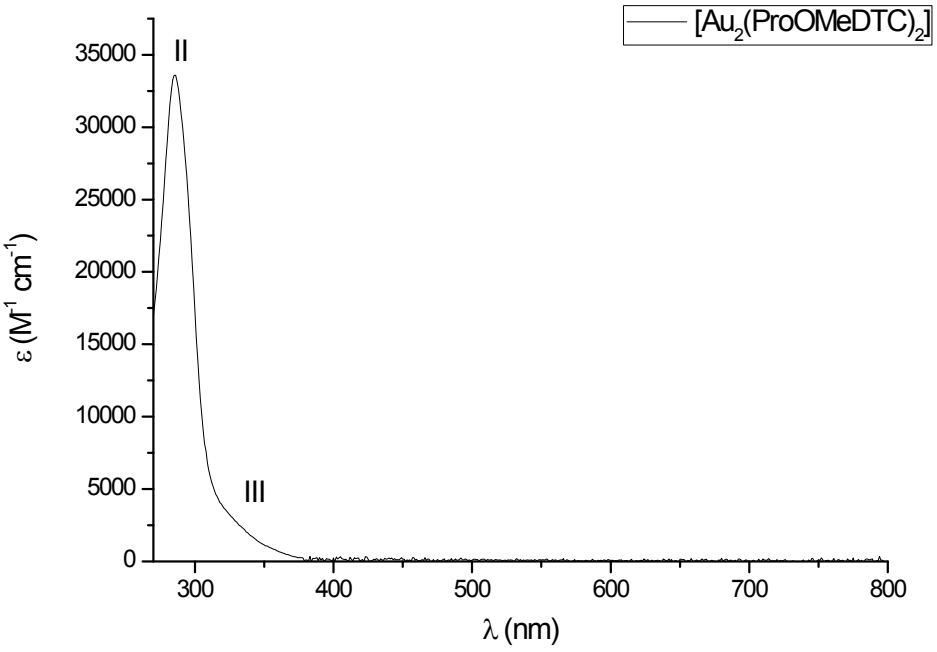

Fig. SI 26 UV-Vis spectrum (DMSO, 25 °C) of bis(L-proline methyl ester dithiocarbamate)digold(I), $[Au_2(ProOMeDTC)_2]$ (**1**).

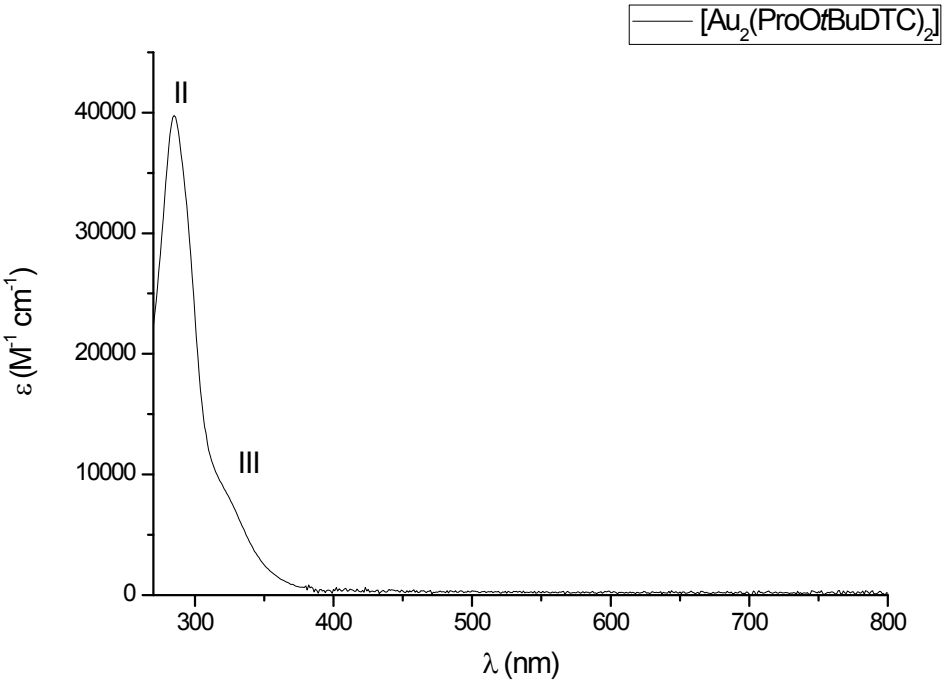

Fig. SI 27 UV-Vis spectrum (DMSO, 25 °C) of bis(L-proline *tert*-butyl ester dithiocarbamate)digold(I), $[Au_2(ProO\mathit{t}BuDTC)_2]$ (**2**).

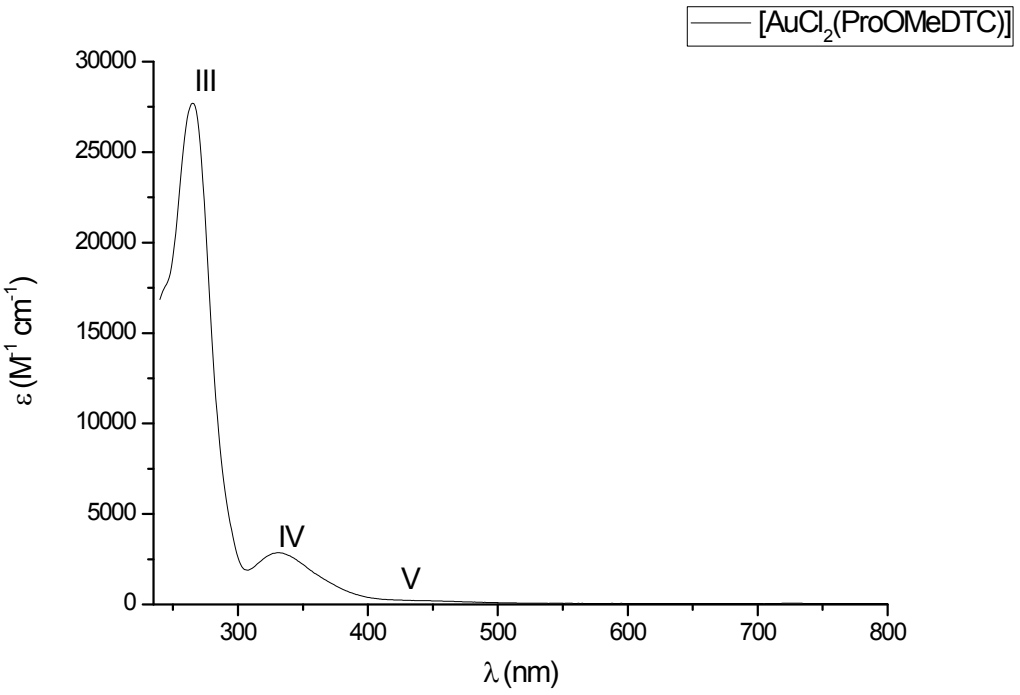

Fig. SI 28 UV-Vis spectrum (CH_2Cl_2, 25 °C) of dichloro(L-proline methyl ester dithiocarbamate)gold(III), [$AuCl_2$(ProOMeDTC)] (**3**).

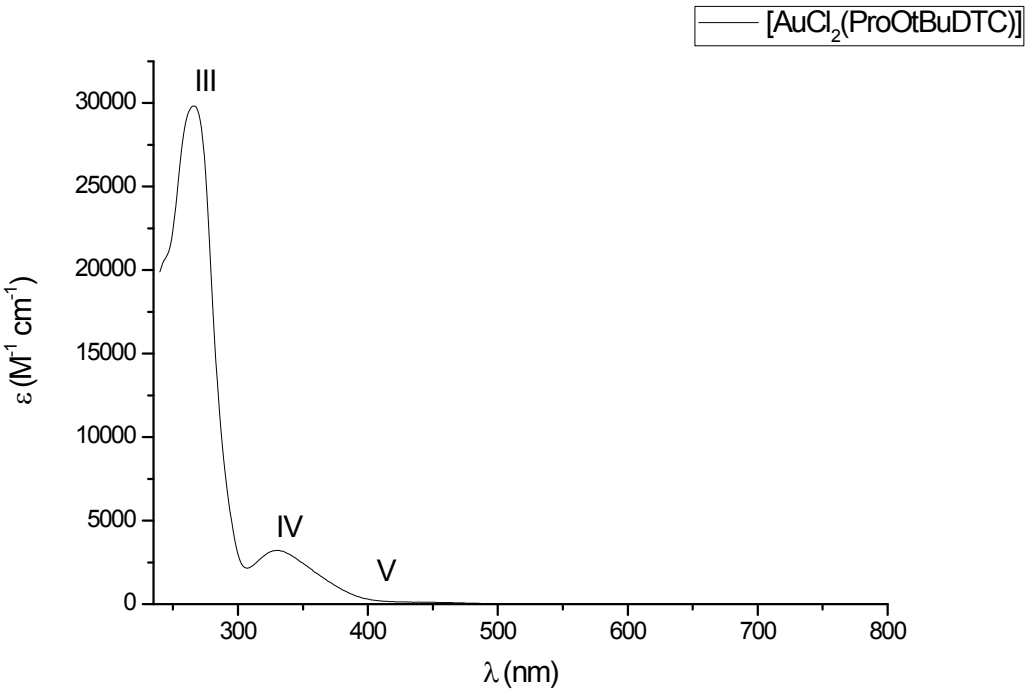

Fig. SI 29 UV-Vis spectrum (CH_2Cl_2, 25 °C) of dichloro(L-proline *tert*-butyl ester dithiocarbamate)gold(III), [$AuCl_2$(ProO*t*BuDTC)] (**4**).

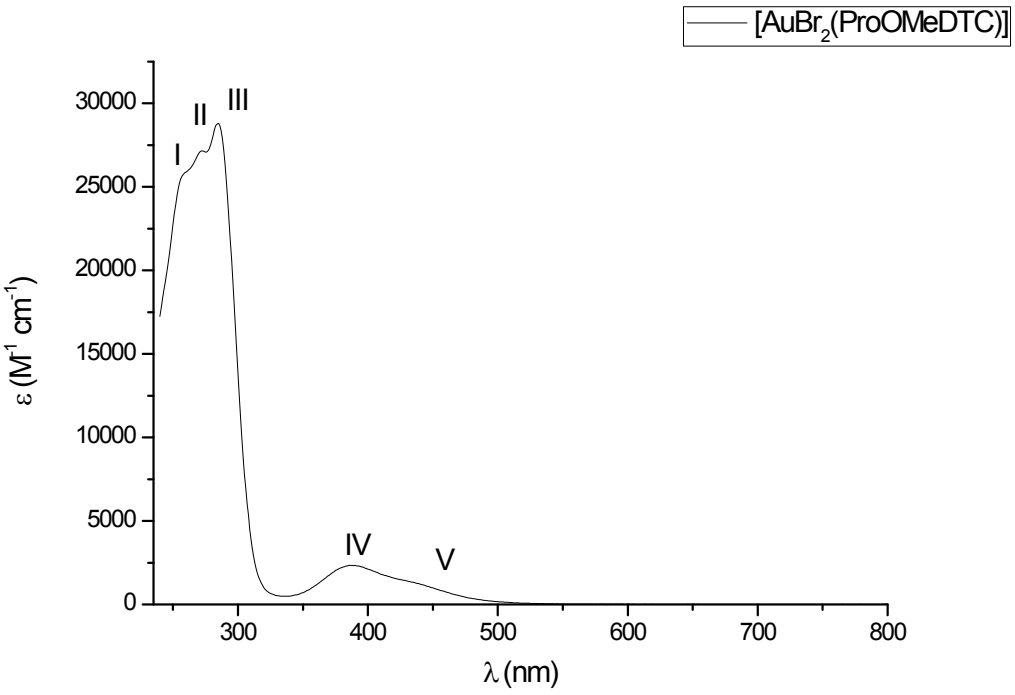

Fig. SI 30 UV-Vis spectrum (CH_2Cl_2, 25 °C) of dibromo(L-proline methyl ester dithiocarbamate)gold(III), [$AuBr_2$(ProOMeDTC)] (**5**).

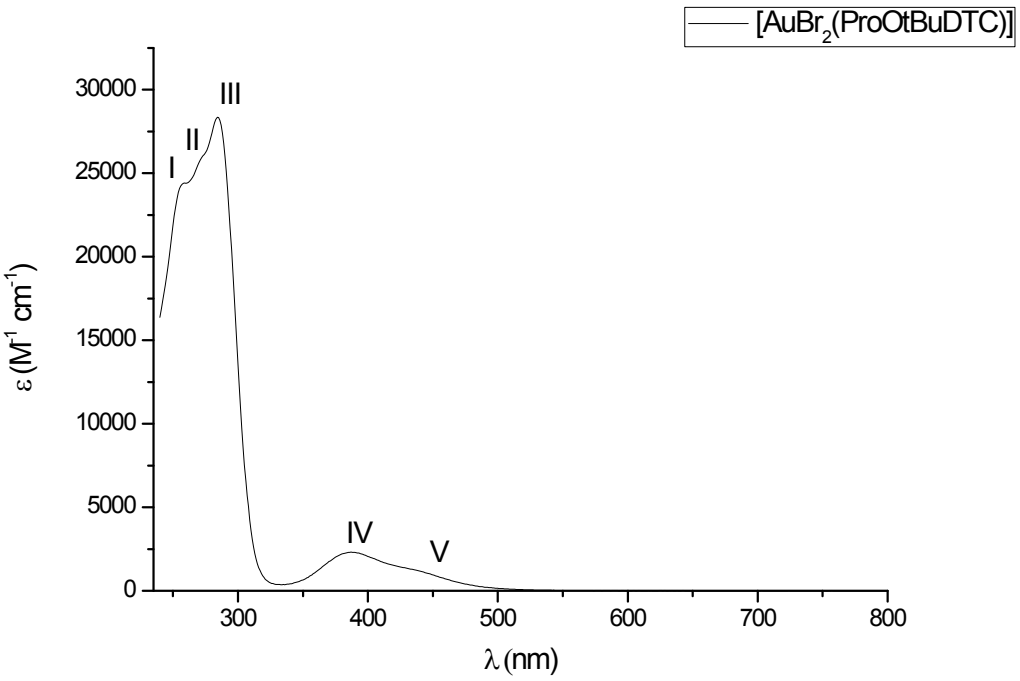

Fig. SI 31 UV-Vis spectrum (CH_2Cl_2, 25 °C) of dibromo(L-proline *tert*-butyl ester dithiocarbamate)gold(III), [$AuBr_2$(ProO*t*BuDTC)] (**6**).

UV-Vis stability studies

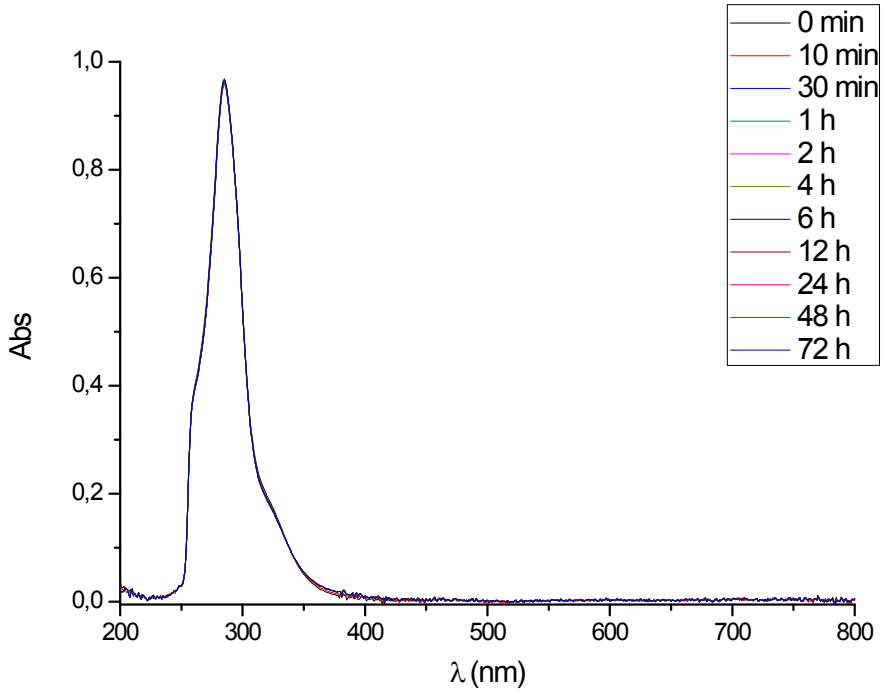

Fig. SI 32 UV-Vis stability study (DMSO/H_2O 1:9, 37 °C, 72 h) of bis(L-proline methyl ester dithiocarbamate)digold(I), [Au_2(ProOMeDTC)$_2$] (**1**).

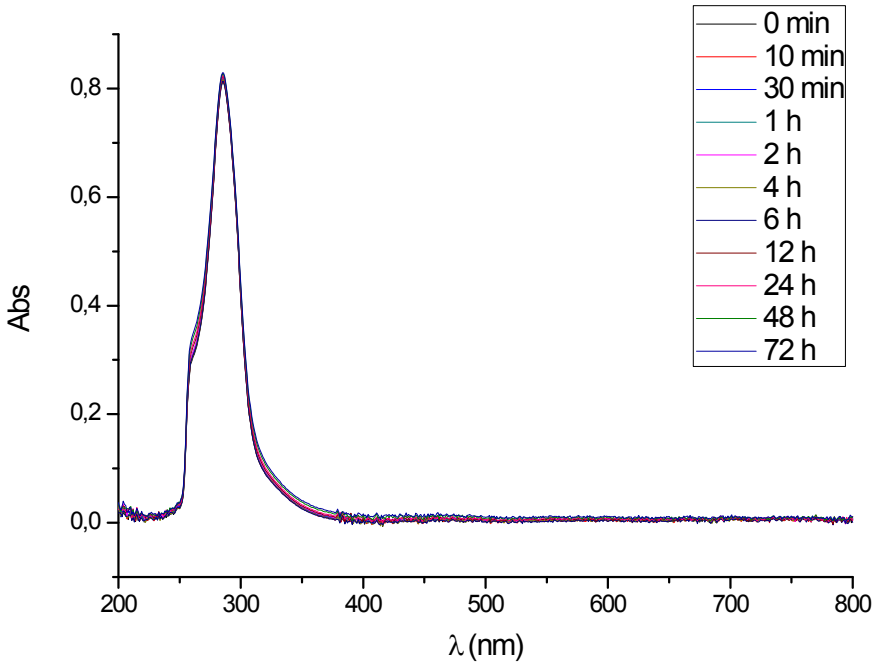

Fig. SI 33 UV-Vis stability study (DMSO/H_2O 1:9, 37 °C, 72 h) of bis(L-proline *tert*-butyl ester dithiocarbamate)digold(I), [Au_2(ProO*t*BuDTC)$_2$] (**2**).

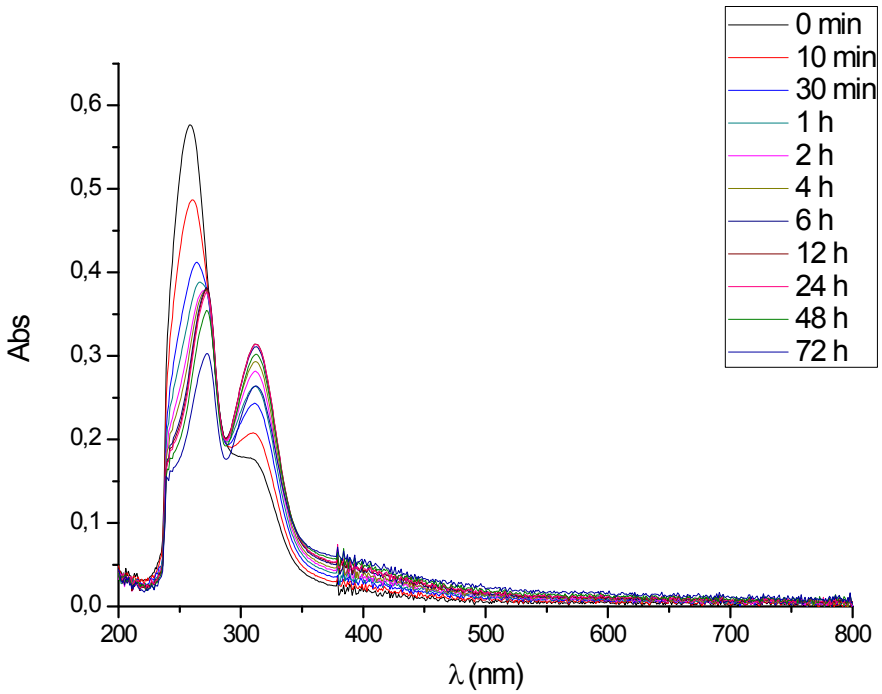

Fig. SI 34 UV-Vis stability study (DMSO/H_2O 1:9, 37 °C, 72 h) of dichloro(L-proline methyl ester dithiocarbamate)gold(III), [$AuCl_2$(ProOMeDTC)] (**3**).

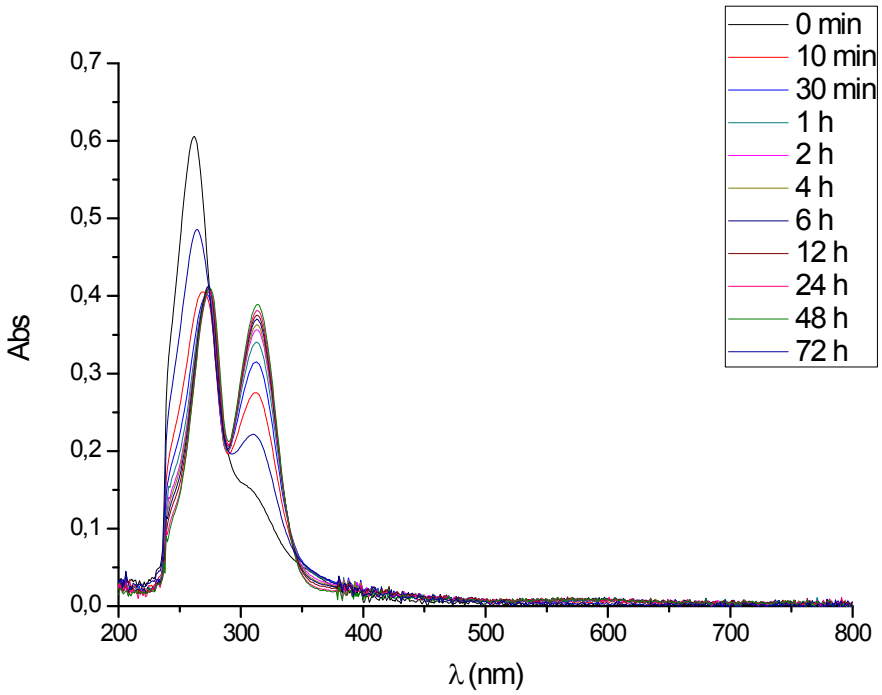

Fig. SI 35 UV-Vis stability study (DMSO/H_2O 1:9, 37 °C, 72 h) of dichloro(L-proline *tert*-butyl ester dithiocarbamate)gold(III), [$AuCl_2$(Pro*Ot*BuDTC)] (**4**).

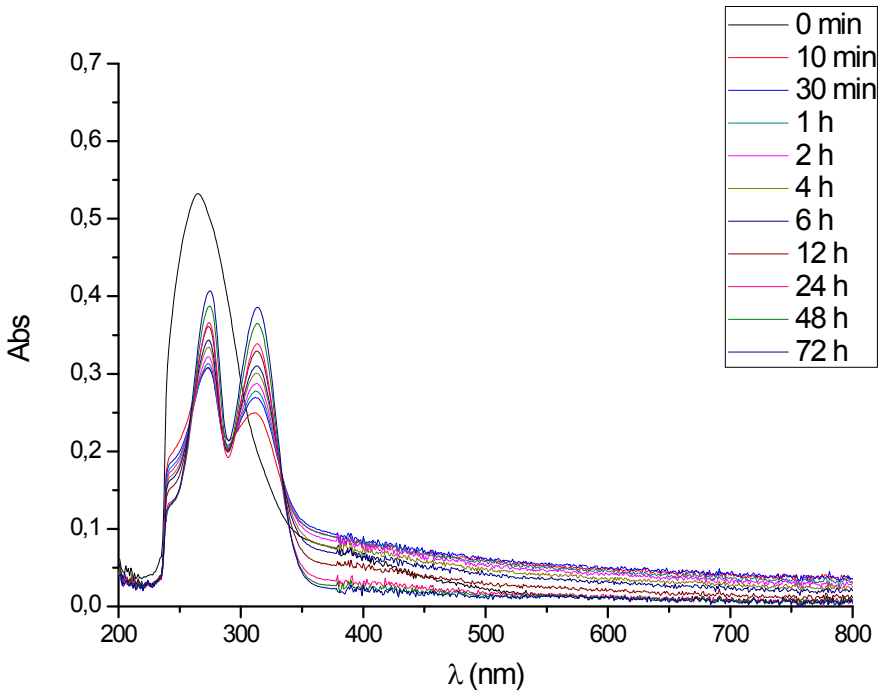

Fig. SI 36 UV-Vis stability study (DMSO/H_2O 1:9, 37 °C, 72 h) of dibromo(L-proline *tert*-butyl ester dithiocarbamate)gold(III), [$AuBr_2$(Pro*Ot*BuDTC)] (**6**).

CD interaction studies

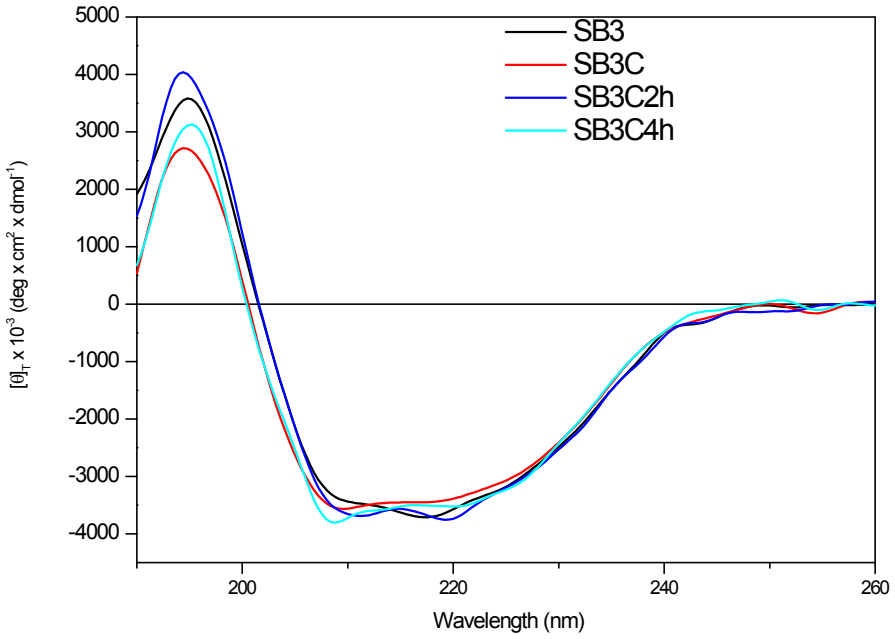

Fig. SI 37 Far-UV CD spectra of Serpin SB3 in presence of complex 3 (SB3C) at different times. [Red: time 0 (SB3C); blue: after 2 h(SB3C2h); light blue: after 4h (SB3C4h)].

	Helix (%)	B-sheet (%)	Turn (%)	Other (%)
SB3	98.0	0	2.0	0.0
SB3C	80.9	0	3.7	15.4
SB3C 2h	91.2	0	1.0	7.8
SB3C 4h	94.3	0	0.0	5.7

Table SI 4 Protein Secondary structure estimation determined using Jasco CD Multivariate SSE software.

Immunofluorescence analysis of SerpinB3 expression

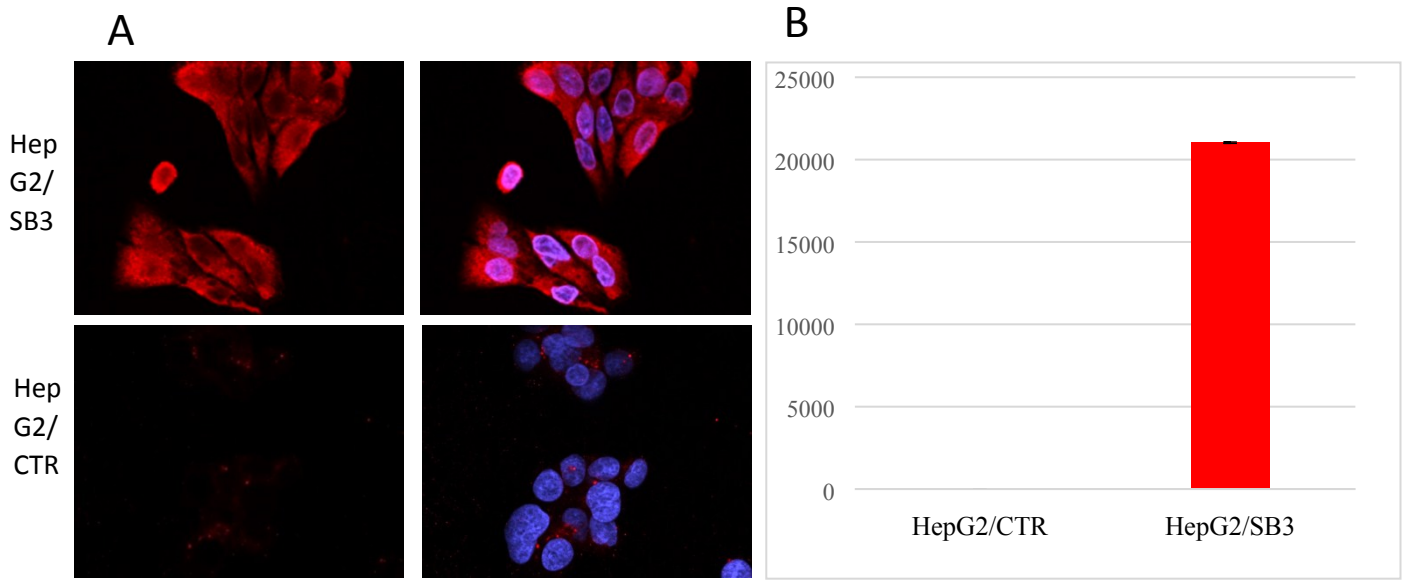

Fig. SI 38 A. Immunofluorescence analysis of SerpinB3 expression (63x objective) in SerpinB3 transfected HepG2 (HepG2/SB3) and in empty vector transfected HepG2 cells (HepG2/CTR). The cells were immunostained with anti-SerpinB3 antibody and the nuclei were counterstained with DAPI. Images were obtained by fluorescence microscopy Axiovert 200 with Apotome 2 (Zeiss). B. Analysis of SerpinB3 transcripts in HepG2/SB3 transfected cells and in HepG2/CTR cells by quantitative real-time PCR (Q-PCR).

Anticancer activity in complete medium containing proline.

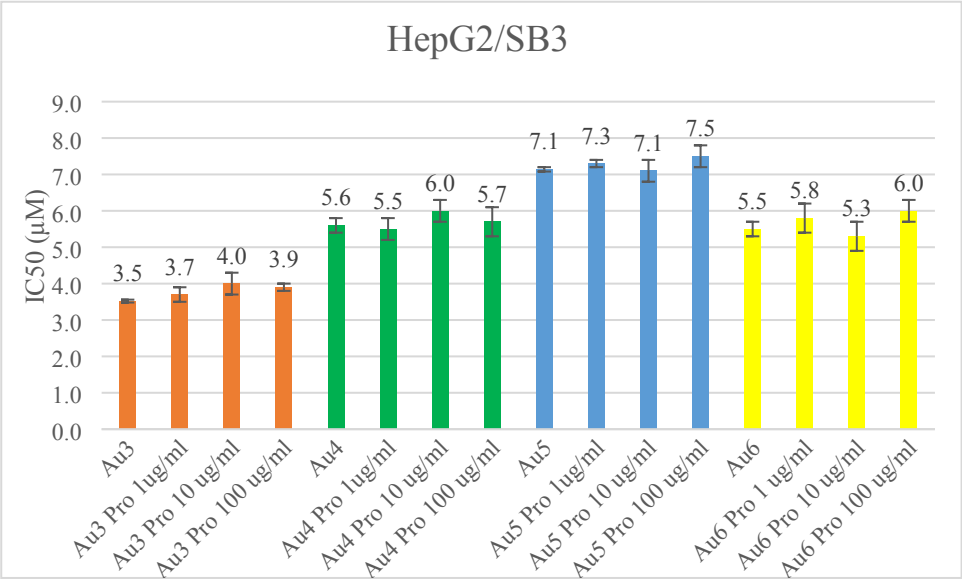

Figure SI 39 IC_{50} values (µM) (concentration of the test agent inducing 50% reduction in cell number compared with control cell cultures) calculated after a 72-h treatment obtained on HepG2/SB3 cell with the compounds 3, 4, 5, 6 also in presence of complete medium containing proline at 1, 10, and 100 µg/ml concentration. Vehicle: DMSO